Cell

Cortical Microtubule Contacts Position the Spindle in *C. elegans* Embryos

Cleopatra Kozlowski,[1] Martin Srayko,[2,3] and Francois Nedelec[1,*]
[1] Cell Biology and Biophysics Unit, European Molecular Biology Laboratory, Heidelberg D-69117 Germany
[2] Max Planck Institute of Molecular Cell Biology and Genetics, Dresden 01307 Germany
[3] Present address: Department of Biological Sciences, University of Alberta, Edmonton T6G 2E9 Canada.
*Correspondence: nedelec@embl.de
DOI 10.1016/j.cell.2007.03.027

SUMMARY

Interactions between microtubules and the cell cortex play a critical role in positioning organelles in a variety of biological contexts. Here we used *Caenorhabditis elegans* as a model system to study how cortex-microtubule interactions position the mitotic spindle in response to polarity cues. Imaging EBP-2::GFP and YFP::α-tubulin revealed that microtubules shrink soon after cortical contact, from which we propose that cortical adaptors mediate microtubule depolymerization energy into pulling forces. We also observe association of dynamic microtubules to form astral fibers that persist, despite the catastrophe events of individual microtubules. Computer simulations show that these effects, which are crucially determined by microtubule dynamics, can explain anaphase spindle oscillations and posterior displacement in 3D.

INTRODUCTION

Correct positioning of the mitotic spindle is vital in determining cell division axes. Interactions between microtubules (MTs) and the cell cortex are often implicated in this process (Manneville and Etienne-Manneville, 2006). Prominent experimental systems include budding yeast and the first division of *C. elegans* embryo (Cowan and Hyman, 2004; Gonczy, 2002; Kemphues et al., 1988; McCarthy and Goldstein, 2006), for which a large number of the molecules involved have been identified. In *C. elegans*, after fertilization of the oocyte, the two pronuclei meet near the posterior of the embryo, migrate to the center of the cell, their nuclear envelopes break down, and the metaphase spindle assembles. As the spindle elongates during anaphase, it also moves toward the posterior of the egg, so that the cell divides asymmetrically. During this time, the spindle oscillates, or ''rocks'' perpendicularly to the A-P (anterior-posterior) axis of the embryo. Notably, the posterior spindle pole oscillates with a larger amplitude than the anterior (Albertson, 1984).

Several models have been proposed to explain spindle posterior displacement (Grill et al., 2001; Grill and Hyman, 2005) and/or oscillations (Grill et al., 2005; Pecreaux et al., 2006). Since both oscillation amplitude and the extent of spindle displacement are determined by cortical polarity, it is possible that both processes are manifestations of a common force-generating activity, originating at the cortex, and acting on astral MTs. To investigate the source of the forces, the spindle was severed using a laser (Grill et al., 2001), which caused the poles to move apart. The posterior pole moved toward the posterior at a higher speed than the anterior pole (Grill et al., 2001). To elucidate the origin of the forces, Grill et al. (2003) used a laser microbeam to fragment the centrosomes. The fragments moved radially toward the cell cortex, suggesting that 'Force Generators' (FGs), widely distributed over the cell cortex, could position the spindle by pulling on astral MTs. From the distribution of speeds of these fragments, it was estimated that approximately 50% more FGs were active on the posterior compared to the anterior pole (Grill et al., 2003).

There is also molecular evidence to suggest that spindle positioning forces are regulated at the cell cortex. The highly conserved PAR proteins (Kemphues et al., 1988), and at least one downstream regulator of spindle positioning, GPR-1/2 (Colombo et al., 2003; Gotta et al., 2003), are required for asymmetric division, and are localized asymmetrically at the cortex during mitosis. In addition, actin and its adaptors preferentially localize to the anterior cortex until the end of metaphase (Hill and Strome, 1988; Munro et al., 2004).

A central focus of the field is to understand how the asymmetrically distributed polarity cues are transduced into pulling forces, and how the FGs exert these forces. The FG could be a complex containing cytoplasmic dynein (Grill et al., 2003; Strome et al. 2001). Such minus-end directed motors anchored to the cortex could pull by 'walking' along astral MTs. Alternatively, FGs might act by capturing shrinking MTs (Cowan and Hyman, 2004). Both mechanisms could result in pulling forces directed toward the cortex. However, in order to explain oscillations, and why these pulling forces do not cause the

spindle to hit the cortex, there must be a 'restoring force' to counteract the cortical pulling. This may arise from pushing forces if the MTs are sufficiently rigid (Grill et al., 2005; Howard, 2006) or from pulling forces (Grill and Hyman, 2005).

MT dynamics influences the orientation and geometry of MT contacts with the cortex, thereby regulating the mechanism of force production and transmission (Dogterom et al., 2005; Inoue and Salmon, 1995). In particular, MT dynamics is likely to affect spindle pole motion, because it determines the number of MTs reaching the cell cortex, where the FGs are located. Thus we decided to analyze the role of MT dynamics using confocal microscopy in two worm strains expressing different fusion proteins. We used a strain expressing α-tubulin tagged with YFP to visualize entire MTs, and EBP-2, a homolog of the TIP tracking protein EB1, tagged with GFP to visualize the growing plus ends of MTs (Srayko et al., 2005). By examining MTs in the cytoplasm and at the cortex, we determined that plus-ends of MTs contact the cortex for about 1 s. We also imaged the posterior pole in a cross-section of the cell, perpendicular to the A-P axis, and found that MTs contact the cortex near the same position during an oscillation cycle. We then reproduced the transverse motions of the posterior pole in 2D simulations, and analyzed its parameters. Next, we simulated two poles connected by a 'spindle' in 3D, and found that two different models, where either there is a higher number of active FGs on the posterior, or stiffer FGs on the anterior cortex, could explain both the posterior displacement and asymmetric oscillations of the spindle. Last, we systematically varied individual parameters, and found that posterior displacement is more robust than pole oscillations, consistent with some experimental conditions that allow spindle displacement in the absence of oscillations (Pecreaux et al., 2006; Schmidt et al., 2005).

RESULTS

Microtubules Contact the Cortex Briefly before Undergoing Catastrophe

In order to build a model based on realistic parameter values, we first observed MT dynamics in the living embryo. MT growth speeds at anaphase were previously reported to be 0.51± 0.02 μm/s, based on imaging of EBP-2::GFP (Srayko et al., 2005). Using spinning-disk confocal imaging of YFP::α-tubulin-expressing embryos, we estimated MT shrinkage speeds to be 0.84 ± 0.16 μm/s (data not shown). MT catastrophe events in the cytoplasm were not quantified but appeared to be rare, since during anaphase, EBP-2::GFP dots seldom disappear before they reach the cell cortex (Srayko et al., 2005). Thus most catastrophe events occur at or very close to the cell cortex.

To quantify MT catastrophe events at the cortex, we first imaged YFP::α-tubulin within an optical section mid-way through the anaphase embryo (longitudinal plane) (Movie S1 in the Supplemental Data available with this article online). We found that MTs exhibited a catastrophe within 1.4 ± 1.1 s after contacting the cortex (n = 17) (Figure 1A). We confirmed these measurements using a hanging-drop mounting method, to examine MTs at the cortex. This method prevents distortion of the native egg geometry, and allows the spindle to oscillate freely. In a single confocal plane, we imaged the inner cortical surface (Movie S2). At anaphase onset, the images contained mostly dots and few lines (Figure 1B and Movie S2), indicating that most of the MTs are perpendicular, rather than at acute angles to the cortex. By telophase, however, the majority of MTs were contacting the cortex laterally (end of Movie S2).

In order to quantify the MT catastrophe rate at the cortex, we measured the time that YFP::α-tubulin-labeled MTs were visible in the confocal plane, within the first 40 s of anaphase onset. We tracked the dots over successive frames (see Figure 1C for number of dots per frame) and calculated a total residency time for each dot. We could fit their distribution by a single exponential of half-life 4.1 ± 0.8 s seconds (mean ± SD; n = 21 fits from 21 embryos, one of which is shown in Figure 1D and Movie S3). We found similar residency times at metaphase (data not shown), which is significantly lower than the residency times previously reported by Labbe et al., (2003). We attribute this discrepancy to the different sample-mounting techniques and image-acquisition parameters used (see Supplemental Data). These observations were confirmed by using EBP-2::GFP embryos (Movie S4), in which residency times are also distributed exponentially (Figure 1D), but with a half-life of 2.1 ± 0.5 s (n = 7 embryos). The shorter times obtained with EBP-2::GFP compared to YFP::α-tubulin likely result from the fact that the former only labels growing MT ends, whereas the latter labels entire MTs (Figure 1E). Considering the ~1 μm optical depth of the confocal microscope we used, a growing MT entering the imaging plane would need about 2 s to reach the cortex (growth speed is ~0.51 μm/s). Measurements made with YFP::α-tubulin embryos also include the time that the MT spends touching the cortex, and about ~1 s for the MT to exit the focal plane after catastrophe (MT shrinkage speed is ~0.84 μm/s). The measurements with EBP-2::GFP, however, only include the time taken for the MT to reach the cortex, as EBP-2 disappears soon after contact (Srayko et al., 2005). Therefore, the time excluding contact is ~3 s for YFP::α-tubulin, and ~2 s for EBP-2::GFP. These are very rough estimates neglecting aster movement, but the duration of contact between MTs and the cortex inferred from this analysis is about 1 s or less (4.1 − 3 = 1.1 s for YFP::α-tubulin; 2.1 − 2 = 0.1 s for EBP-2::GFP), which is consistent with the average residency times obtained by lateral imaging (1.4 s).

Given this short MT contact time, we propose that the FGs (which may, or may not be a complex containing a molecular motor) could act briefly on shrinking MTs near the cortex, in a "touch-and-pull" mechanism, perhaps by converting MT depolymerization energy into a pull on the cortex (Figure 1E).

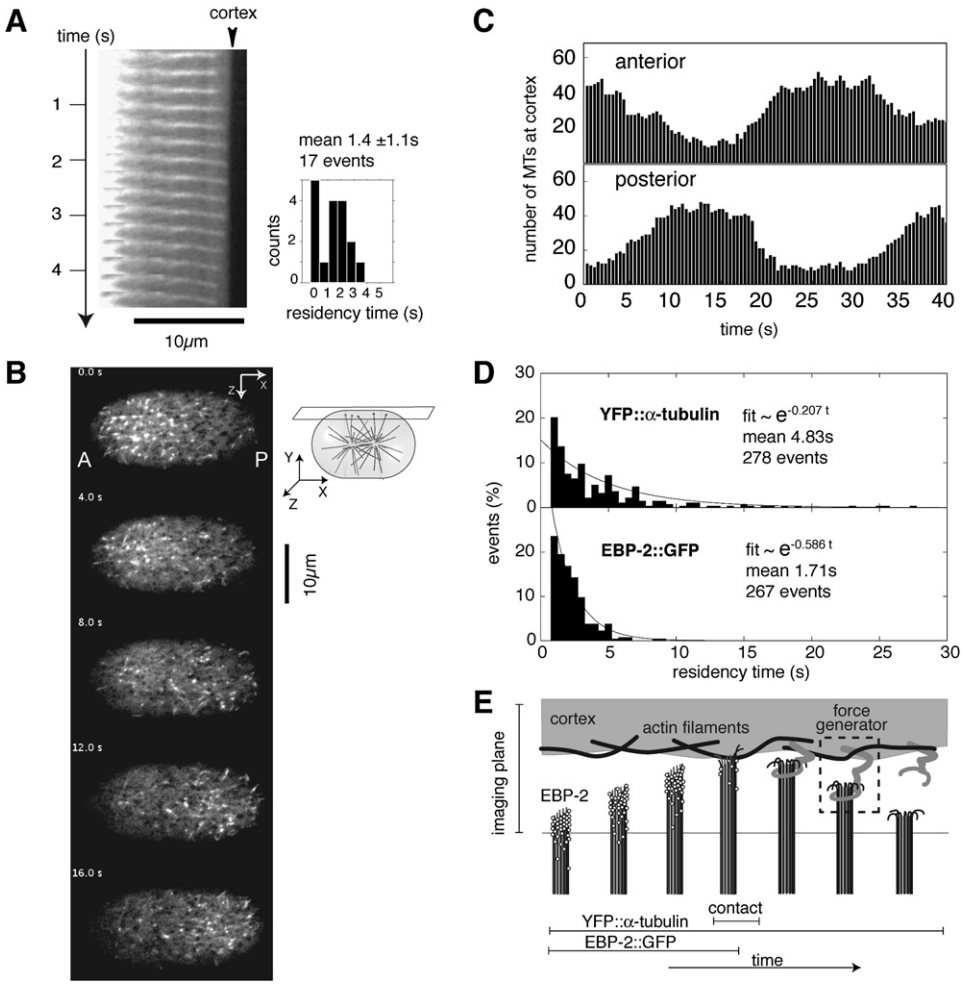

Figure 1. Microtubules Contact the Cortex Briefly before Undergoing Catastrophe

(A) Kymograph of a MT fiber approaching the cell cortex in a YFP::α-tubulin embryo at anaphase (left). Black arrowhead indicates the cell cortex. The histogram (right, binned at 0.7 s intervals) shows the distribution of contact times for 17 events.

(B) We define the x-axis as the A-P (longitudinal) axis of the embryo, and the y- and z-axes arbitrarily in the transverse plane. Here, a slice parallel to the longitudinal XZ-plane and near the cortex is imaged in YFP::α-tubulin embryos.

(C) Number of MTs quantified as a function of time, for the anterior and posterior sides of the embryo shown in (B).

(D) Anaphase residency times in a single YFP::α-tubulin or EBP-2::GFP embryo. Histograms (binned at 0.5 s intervals) are distributed exponentially for both strains. The least square fit to a single exponential are indicated (line), together with deduced mean residency times.

(E) Model of a MT contacting the cortex. EBP-2 is located at the tips of growing MTs, but disappears when MTs reach the cortex. There the MT has a high probability of being captured by a force generator, which pulls when the MT depolymerizes. Structural components of the cell cortex, including actin, likely contribute to the rigidity of the MT-cortical interaction. The residency times that are measured using cortical imaging of YFP::α-tubulin or EBP-2::GFP embryos are indicated.

Dynamic Microtubules Associate with Each Other to Form Persistent Astral Fibers

Since the cross-sectional radius of an average embryo is 15 μm, an average MT growing at ~0.5 μm/s and shrinking at ~0.8 μm/s would require about 30 s to grow from the pole to the cortex, plus a second of residency at the cortex, and 20 s to shrink back to the pole. Given the oscillation period of approximately 25 s, it was surprising that YFP::α-tubulin embryos appear to have persistent "fibers" that are present throughout the period of oscillation, or even longer (Figure 2A). Observations of EBP-2::GFP dots indicated that MTs often grow along the trajectory taken by another MT (Movie S5). By imaging YFP::α-tubulin, we also noted that such fibers could branch off from each other (Figure 2B). These two observations indicate that the fibers could be groups of MTs constantly growing and shrinking along each other, but loosely associated. After the longest MT in the fiber depolymerizes, another growing MT could overtake it, in an effective "rescue" event of the fiber (Figure 2C). As a consequence, a fiber would appear to be persistent.

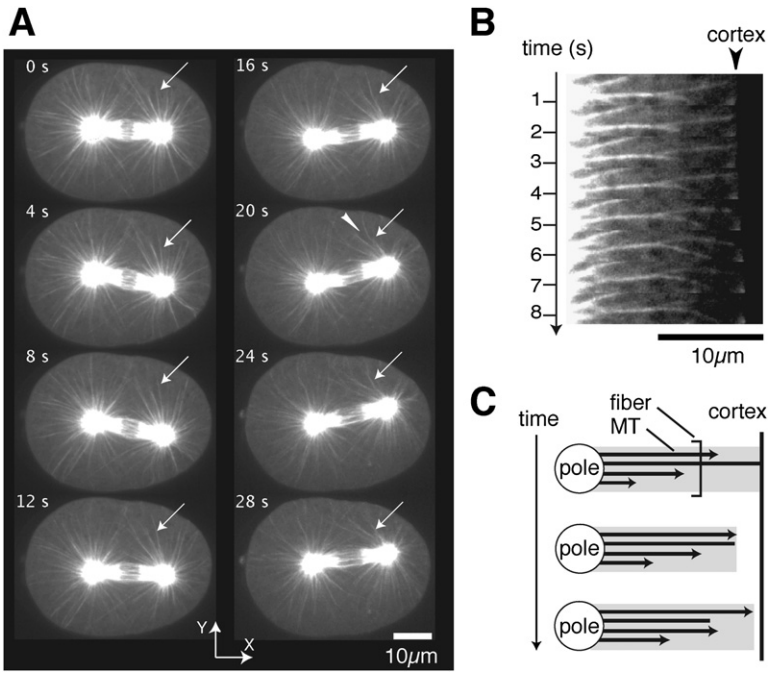

Figure 2. Microtubules Are Associated in the Cytoplasm

(A) Time-lapse series of a YFP::α-tubulin embryo imaged during anaphase oscillations. The white arrows point to a group of MTs, or a "fiber" present for the entire length of the movie (28 s). Sometimes the fiber bends considerably (white arrowhead).

(B) Kymograph of a region from an embryo imaged as in (A), where MTs branch off of a 'fiber'.

(C) Model of how dynamic MTs growing along each other could be seen as a persistent fiber. The longest MT starts shrinking (blunt end), but the first growing MT (arrows) catches up and "rescues" the fiber.

Microtubule Fibers Contact the Cortex at Fixed Positions

The MT "fibers" were also evident in embryos imaged in the transverse plane from the posterior end (Figure 3A), where the MTs radiated from the posterior pole toward the cortex (Movie S6). Importantly, as the aster moved during anaphase, the distal tips of MT fibers remained as if fixed near the cortex throughout the oscillation (Figures 3B, 3C, and S1). Concurrently, the angles at which MTs contact the cortex vary in such a way that a portion of the FG-mediated pulling force would be directed toward the center of the cell (Figure 3B). This prompted us to consider fiber flexibility in the model.

Correlation between Aster Motion and Contact Frequency

Imaging of the same transverse section with EBP-2::GFP allowed a closer examination of the behavior of the growing ends of MTs as the aster oscillates (Figure 3D). To highlight the motion of MT plus-ends over time, we superimposed every 6 successive frames (2.4 s) from one movie (Figure 3E). In these projections, MT plus ends appeared as lines if the MT grew in the same direction as aster motion, *i.e.,* where MT ends moved at a speed equal to the sum of the aster speed and MT growth (Figure 3B). On the other hand, MTs growing in the opposite direction appeared as stationary dots, because the MT growth speed is close to the pole speed. This indicates that, during pole movement, many more MTs reach the approaching cortex than the receding cortex.

This explains a curious observation made when imaging the cortex. In 7 out of 21 YFP::α-tubulin embryos, we observed time-dependent oscillations in the number of dots (MT ends) appearing on the anterior and posterior cortex (Figure 1B and Movie S3). Like the spindle pole oscillations, the MT-end density also alternated in opposite phase with respect to the anterior and posterior regions of the cortex (Figure 1C). However, when averaged over several oscillation cycles, there was no statistically significant difference in the overall number of MTs contacting the anterior or posterior cortex (Experimental Procedures). This oscillation in dot number had a periodicity of approximately 25 s (Figure 1C), similar to that of spindle oscillatory motion, and we reasoned that this should occur when the spindle oscillated perpendicularly to the imaging plane. Together, these observations suggest that more MT contacts are made on the side of the cortex that is approached by the aster than on the receding side. If MT catastrophes triggered at the cortex are linked to brief pulling events in a touch-and-pull mechanism, the forces could be determined by the frequency of MT contacts. Consequently, a positive feedback would be created between the pole motion, and cortical forces. Furthermore, the feedback would be maximal because the poles move at speeds comparable to MT growth.

2D Simulations of Oscillations

Using insights gained from microscopy, we built a simple model of the posterior pole oscillations using cytosim (Nedelec, 2002) to simulate a single aster with 300 "fibers", in a 2D circular cell of 15 μm radius (Experimental Procedures). Each fiber represents a group of several MTs (on average 6 and up to 15), which grow and shrink independently, but bend together when the aster deforms, as observed in vivo. In keeping with our in vivo observations, the simulated MTs undergo a catastrophe rarely in the

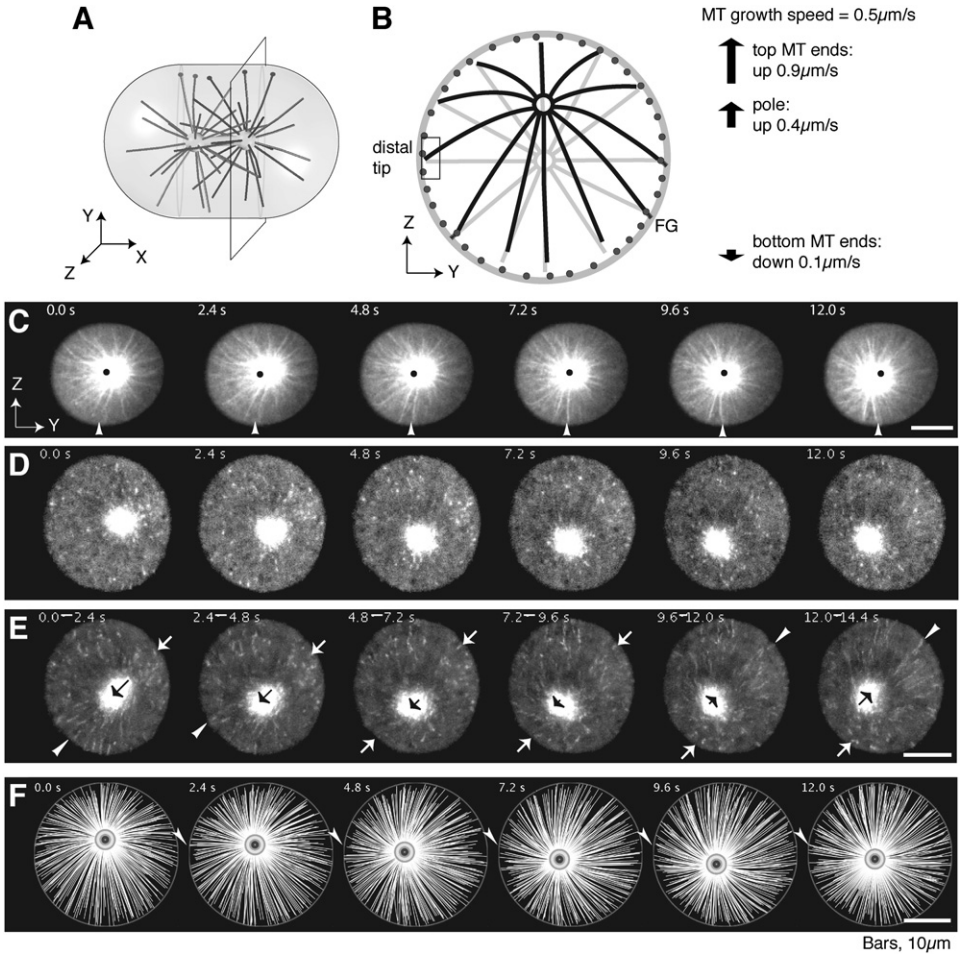

Figure 3. Posterior Pole Movement in the Transverse Plane

(A) For imaging poles in the transverse plane, a slice perpendicular to the longitudinal axis of the embryo and containing the posterior pole is imaged. This section is invariant by rotation around the x axis.

(B) Aster in its initial position (gray) and off-center (black). Fibers bend and contact the cortex always at approximately the same position. When the aster displaces, the direction of pulling forces produced on MT tips turns toward the center. If the aster is moving upwards at 0.4 μm/s, and MTs are growing at 0.5 μm/s, then the ends of MTs extending upwards move at a net speed of 0.5 + 0.4 = 0.9 μm/s, whereas the MT tips extending downwards move at a net speed of 0.5 − 0.4 = 0.1 μm/s.

(C) A posterior pole in an anaphase YFP::α-tubulin-expressing embryo imaged in the y-z plane. Black dots indicate the center of the cell. Note that even though the aster is oscillating, the MT plus-ends contact the cortex in the same location (compare with the white arrowheads which indicate the same position on the cortex in all frames).

(D and E) Posterior pole of an EBP-2::GFP-expressing embryo imaged in the y-z plane. The time-lapse shown in (D) is processed in (E) by taking the maximum value over 2.4 s for each pixel. Black arrows indicate the direction and magnitude of speed of the aster motion. EBP-2::GFP appears as lines (white arrowheads) in the projections when MTs are growing in the direction of pole motion. Dots are observed (white arrows) when the MTs are growing in the opposite direction of the pole.

(F) Simulation of an aster in 2D. MT plus ends contact the cortex always at the same location (white arrowheads) as a consequence of the flexibility of the MTs and the viscosity of the cytoplasm.

cytoplasm (rate∼0.01/s), but frequently while touching the cortex. Fibers reaching the cortex also have a chance of being captured by a FG (*attachment rate is* ∼5/s), which generates a pulling force when the fiber shrinks.

Parameter values for the simulation were set to measured values when possible, or varied across a reasonable range (Table 1). We first generated random parameter sets, and observed the behavior of an aster initially placed in the center of the circle. We found that many combinations caused the aster to either hit the cortex without a single oscillation, or to remain stably at the center. However, in 2D about 10% of the combinations were able to reproduce motions similar to those of the posterior spindle pole in the embryo (compare Figures 3C and 3F, and Movies S6 and S7). The motions included oscillations (alternating movement along a single axis) and gyrations (rotations around the center), and mostly irregular combinations of both. To obtain a simple and informative indicator of the

Table 1. Parameter Values in the Reference Simulations

Description	Value	Note
Simulation-Specific		
Iterations	15,000	Total time simulated = 150 s.
Time step (s)	0.01	
Cell		
Viscosity (pN s/μm^2)	1	(Daniels et al., 2006) Varied 0.1–2
Confinement elasticity (pN/μm)	100	[a]
Sizes (μm)	30x30x50	A spherocylinder, see text for description[a]
Microtubules		
Fiber rigidity (pN μm^2)	120	(Dogterom and Yurke, 1997) Varied 1–500
Growth rate ($\mu m\ s^{-1}$)	0.51	(Srayko et al., 2005) Varied 0.0–2.0
Shrinkage rate ($\mu m\ s^{-1}$)	0.84	This study. Varied 0.0–2.0
Cytoplasm catastrophe rate (s^{-1})	0.01	[a]
Cytoplasmic rescue rate (s^{-1})	0	[a]
Cortical catastrophe rate (s^{-1})	5	This study. Varied 1–10
Sensitivity of growth to force (pN)	1.67	(Dogterom and Yurke, 1997)[a]
Nucleation rate per MT (s^{-1})	0.05	25 new MTs per second per pole[a]
Max. number of MT per fiber	15	[a]On average, 6 MTs per fiber
Number of fibers per pole	300	[a]
Force Generators		
Detachment rate (s^{-1})	0.003	Varied 0–0.004
FG/cortical rigidity (pN/μm)	370[b]	Varied 1–2000
Characteristic force (pN)	26 in 2D and 28 in 3D	(Grishchuk et al., 2005) Varied 1–100
Attachment rate (s^{-1})	5[c]	Varied 0–10
Asymmetry (% decrease of cortical elasticity, or % increase in FG attachment rate on posterior)	50%	Varied 0%–100%
Spindle (3D Only)		
Initial length (μm)	8	After 150 s (end of simulation) spindle length is 18 μm[a]
Elongation rate (μm/s)	0.070	

[a] Not varied.
[b] In the 3D model where the polarity affects *FG/cortical rigidity*, rigidity is 370 on the posterior half, and 560 on the anterior half. In 2D, the rigidity is 370.
[c] In the 3D model where the polarity affects *FG attachment*, this rate is 5 on the posterior half, and 3.2 on the anterior half, and the rigidity is 220 everywhere. In 2D, the rate is 5 as the posterior is simulated.

motion of the aster, its speed was averaged over the entire simulation period, or until the aster hit the cell cortex, if it did (Figure 4A). The mean speed is higher than 0.2 μm/s only if the aster oscillates or gyrates, as in the real embryos. Lower values indicate irregular motions or unnaturally slow oscillations. We thus define this speed as the "oscillation speed", and use it as a measure of oscillations throughout this manuscript.

By examining the mechanism by which the aster oscillates, we found that pulling forces alone are sufficient to maintain stable oscillations (Figure S2), and that the restoring force in our model is linked to deformations of MT fibers extending laterally to the oscillation axis (Figure S3). As seen in the embryo (Figure 3C), when an aster moves off-center, the orientation of MT tips at the cortex are such that pulling forces tend to restore it to its initial position. Yet, the simulation reveals that if the parameters are such that the pole moves faster than the MT growth rate (Figure 4A), the pole will hit the cortex. This is because too few lateral MTs make contact with the receding cortex, and consequently no restoring pulling forces are produced. A key feature of this postulated restoring-force

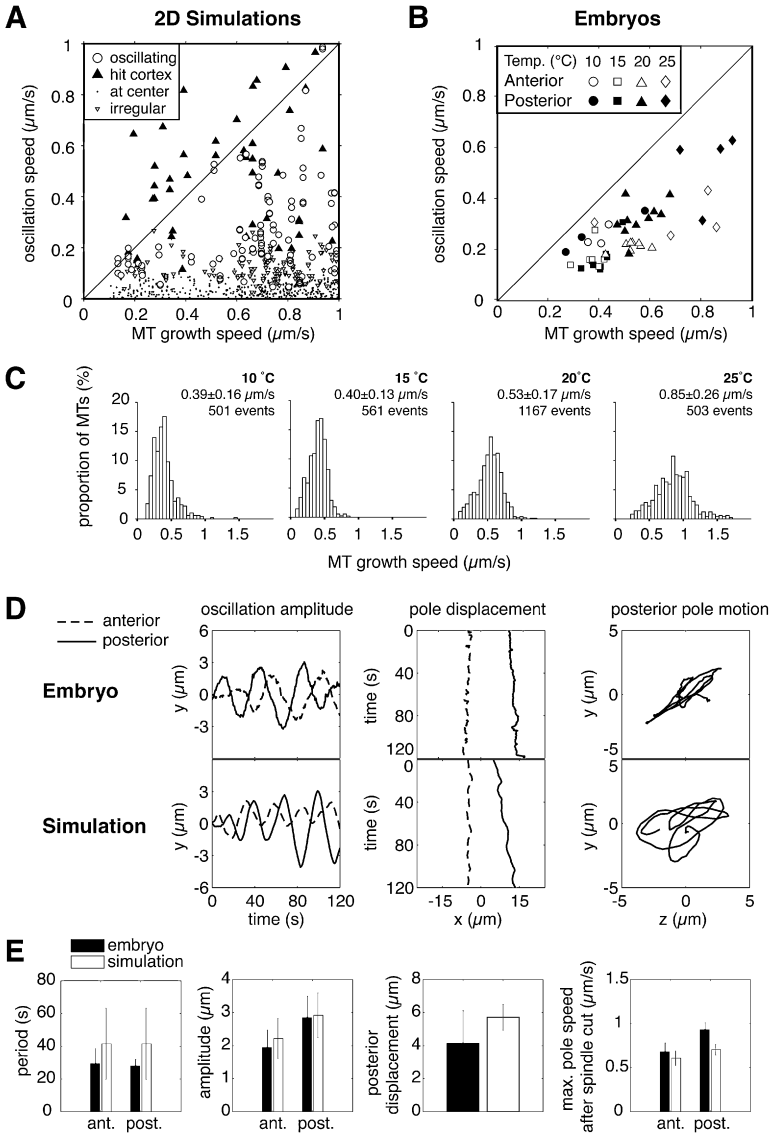

Figure 4. Comparing Spindle Movements in Embryos and Simulations

(A) Each symbol represents a 2D simulation of an aster in a circular section of the cell, and is positioned according to the parameter that defines the MT growth speed, and the resulting oscillation speed (see text). Several parameters are varied simultaneously in 1000 simulations (see Table 1 for parameters): *cytoplasmic viscosity, FG/cortical rigidity, MT growth rate, MT shrinkage rate, FG force, FG attachment rate, FG detachment rate, MT rigidity, MT catastrophe rate*. The symbol indicates the qualitative motion of the aster as judged visually. Circles (○): asters oscillated or gyrated without hitting the cortex. Solid triangles pointing up (▲): asters hit the cortex after oscillating at least once. Open triangles pointing down (▽): asters moved irregularly and without sustained motion in any direction. Dots (.): asters stayed near the center of the cell.

(B) Average anterior and posterior pole speeds and MT growth speeds for each pole were measured in EBP-2::GFP embryos, imaged at various temperatures. Pole speeds are always slower than MT growth speed.

(C) MT growth speeds at anaphase, measured at different temperatures, using EBP-2::GFP embryos. The histograms are binned at 0.05 μm/s. Note the temperature-dependent increase in MT growth speed.

(D) Experimentally tracked spindle pole trajectories (top) compared to simulations (bottom). Panel 1 shows the component of pole motion perpendicular to the A-P axis over time, where 0 indicates the A-P axis. Panel 2 shows the separation of the asters along the A-P axis over time, where 0 indicates the center of the cell. Panel 3 shows irregular motion of the posterior pole in the y-z plane.

(E) Characteristics of pole trajectories from 15 wt embryos (black bars) and 100 simulations (white bars), for the model where the *FG/cortical rigidity* is varied. Mean and standard deviations of the oscillation period, the amplitude, the posterior displacement of the center of the spindle, and the speed of asters moving apart after spindle severing (in this case, experimental values are from Grill et al., 2001).

mechanism is that the oscillations can be sustained only if pole speed is lower than MT growth rate.

To test whether we could observe this relationship in vivo, we imaged EBP-2::GFP embryos at temperatures between 10 and 25°C, a range at which embryos develop (data not shown), and compared MT growth and oscillation speed (Figure 4B). Despite considerable variation in MT growth rates at the different temperatures (Figure 4C), the oscillation speed was always slower than the MT growth speed, but interestingly, only slightly slower. This suggests that the posterior pole oscillates at the maximum velocity predicted by our oscillation model.

Next, we performed a ''parameter sensitivity analysis'', with two ''reference'' parameter sets that produce oscillations. They were selected for high oscillation speed, and low probability of the aster hitting the cortex, in order to match the conditions observed in the embryo. The sensitivity to a parameter was measured by running 100 simulations in which only this parameter was varied, and the resulting oscillation speed was recorded. Since different reference sets gave qualitatively similar results, we show the results for only one of them in Figure S4. With this reference set, the aster hit the cortex in 8.4% of cases (note: this did not occur in 3D simulations; see Discussion). We found that increasing the *FG attachment rate* or *FG force* increased the oscillation speed, while increasing *FG/cortical rigidity* (a parameter that incorporates the combined stiffness of the FG and cortex) or *FG*

detachment rate decreased the oscillation speed of the pole (Figure S4).

3D Simulations Reproduce Spindle Positioning in a Polarized Cortex

From the above results, we tested whether we could reproduce the posterior displacement of the spindle as well as the larger oscillations of the posterior pole, by simulating the embryo in 3D. We reasoned that setting a parameter that affects pole speed to different values on the anterior and posterior half-cortices would achieve this. Indeed, previous studies suggested that *FG attachment rate*, and *FG/cortical rigidity* should be tested. For instance, higher *FG attachment* rates could arise either from a larger number of active FGs at the cortex, as in the model of (Grill et al., 2003), or from a higher affinity of the FG for MTs. Likewise, higher *FG/cortical rigidity* could arise from changes to the mechanical property of the cortex, which could, for instance, be determined by the concentration of actin filaments or the activity of their adaptors (Hill and Strome, 1988).

Thus, we extended the model to three dimensions, and simulated two asters for a total of 150 s, including a stabilization period of 30 s, followed by 120 s simulating anaphase. The embryo was modeled as a cylinder capped with two hemispheres, so that the total length was 50 μm, and its width 30 μm. A spindle connecting the two poles is represented as a rigid mechanical element placed parallel to the A-P axis at the center of the cell, which elongates at a constant rate. The same assumptions for MTs, fibers and FG behavior were used as in the two-dimensional model, except that either *FG attachment rate* was set 50% greater, or *FG/cortical rigidity* was set to be 50% less on the posterior half of the cortex, compared to the anterior half (Table 1). Because both models behaved in a very similar way, we present only the data from the model where *FG/cortical rigidity* was altered in Figures 4 and 5 (see Figure S5 for the results of the model where *FG attachment rate* is varied).

We first tested whether our simulation reproduced the movements of the spindle in vivo. To allow quantitative comparison to be made, spindle pole trajectories were measured from wild-type embryos, from longitudinal and transverse views. The simulated and real oscillations in the longitudinal view were similar in amplitude and frequency (Figures 4D and S5A, and Movie S8). The posterior displacement in the simulation after 150 s was similar to that measured at the end of anaphase in vivo. In the transverse view, irregular oscillations, which are mixtures of gyrations and radial oscillations, were also reproduced (Movie S9). Moreover, the motion of the spindle poles in the simulation was quantitatively similar to what was found in 15 wild-type embryos (Figures 4E and S5B). Yet the oscillation periods in silico had a larger standard deviation than in vivo (see discussions for possible reasons). We also simulated the spindle-severing experiment (Grill et al. 2001) by removing the link between the poles during the oscillations, with results similar to what has been measured in vivo (Figure 4E). We could also reproduce the contact density of MTs (Experimental Procedures) and the cortical MT residency times observed with YFP::α-tubulin (Movie S10) and EBP-2::GFP (data not shown).

Finally, under some conditions (low temperature, e.g., below 10°C and through RNAi-mediated knockdown of proteins involved in cortical force generation) oscillations are reduced or do not occur even though the early embryo develops normally (data not shown and Pecreaux et al., 2006). In contrast, A-P positioning, is likely to be more resilient to environmental variations, because it is essential for asymmetric division. To test whether a difference in robustness is also present in the model, we performed a parameter sensitivity analysis in 3D, by monitoring the speed of the posterior pole motion and the posterior-directed shift of the mid-zone along the A-P axis after 150 s. When *FG attachment rate* or *FG/cortical rigidity* was decreased, oscillations were lost more quickly than spindle displacement (Figures 5 and S5C). When MT growth or shrinkage speeds were increased to 50% more than in the reference set, the mean pole speed dropped, but the spindle displacement was largely unaffected. Similarly, oscillations were highly sensitive to the parameter *FG detachment rate*, but the spindle still displaced toward the posterior. Therefore, pole oscillations are more sensitive to parameter variation than spindle displacement. The simulations from the sensitivity analysis are available online at www.cytosim.org.

DISCUSSION

Coupling Microtubule Depolymerization to Pulling Forces

Measurements of MT dynamics at the cell cortex and in the cytoplasm led us to propose a model in which pulling forces are generated at the cortex by FGs that remain attached to depolymerizing MT ends. The forces that FGs exert in our simulation match the in vitro measurement of ~50pN produced by shrinking MTs (Grishchuk et al., 2005). We favored this model whereby FGs act predominantly as adaptors at MT tips, after considering the brevity and end-on configuration of most MT-cortical contacts during anaphase, and because the force from a single dynein is limited to 7-8 pN (Toba et al., 2006), but these considerations do not exclude that there may be a contribution from motor activity as well. Depolymerization adaptors (which may also be motors, but not function as such) are found in other organisms: for example Kip3 in budding yeast (Adames and Cooper, 2000; Gupta et al., 2006). This kinesin moves to the MT plus-end where it promotes catastrophe upon cortical contact, producing a pulling force. Dynein has also been implicated in pulling by inducing MT catastrophes at the cortex (Carminati and Stearns, 1997). As the increase in catastrophe frequency at the cortex seems too high to result from force alone (Janson et al., 2003), it is an attractive idea that depolymerization is triggered by the adaptor itself.

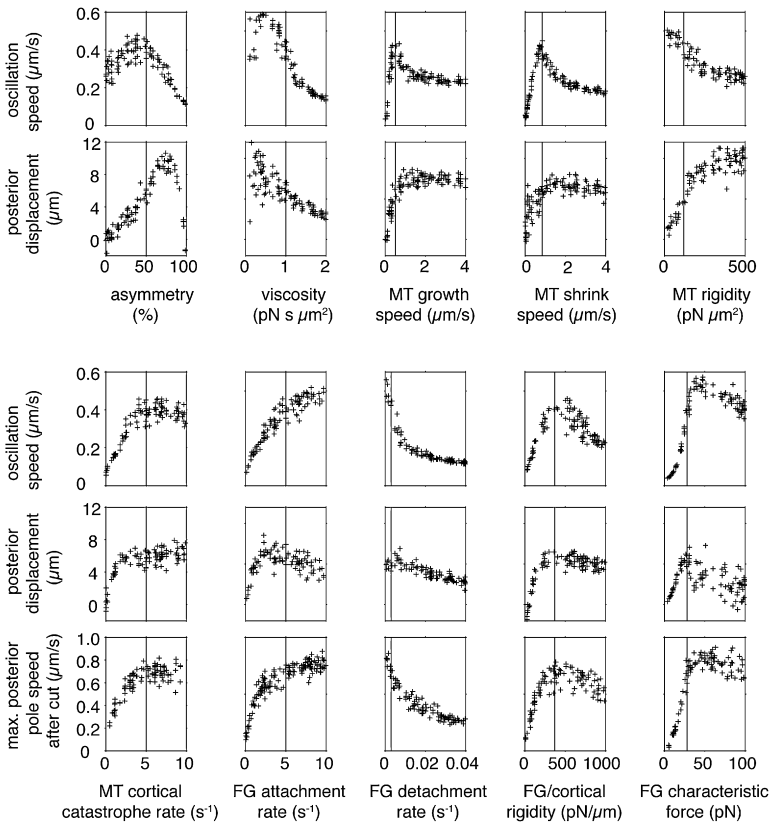

Figure 5. 3D Parameter Sensitivity Analysis

Results from a parameter sensitivity analysis in 3D, in which the *FG/cortical rigidity* is higher on the anterior than on the posterior. In each graph, only one parameter is varied, and each cross (+) represents a single simulation. The X-coordinate indicates the value of the parameter that was varied from its reference value (vertical line). The Y-coordinate indicates the resulting oscillation speed, posterior displacement (measured as shift of spindle mid-zone) and for 5 parameters, the speed of the posterior pole after simulated spindle severing.

Model of Oscillations

Our model of spindle pole oscillations depends on the interplay between pole motion and MT growth and shrinkage rates. MT growth determines when MTs reach the cortex, and reaching the cortex induces catastrophe. In addition, MTs that reach the cortex pull the aster toward the cortex, which, in turn, increase the frequency of more MTs reaching the approaching cortex. Such feedback is always expected for a dynamic aster in confinement (Howard, 2006), and would in the absence of a restoring force lead the aster to crash into the cortex. Restoring forces in our model arise from pulling, as in (Grill and Hyman, 2005), but in a different manner. Their model assumes that MTs are straight and at fixed angles to each other, and that the number of cortical FGs are limiting compared to MT number. Based on our observations that fibers persist throughout oscillations, and that these fibers bend and contact the cortex at approximately fixed positions, we propose that MT fibers that extend perpendicular to the axis of pole motion provide a sufficient restoring force, even when the cortical FGs are in excess. Simulated asters hit the cortex occasionally in 2D, but never in 3D, because there are more 'lateral' fibers in 3D.

Asymmetry

We found that in 3D, asymmetric spindle movement could arise from a differential distribution of *FG/cortical rigidity* or *attachment rate* of FGs on the posterior compared to the anterior half-cortices. Other factors, such as asymmetry of *cortical catastrophe rate*, or *FG detachment rate*, could also give asymmetric spindle positioning and oscillations (data not shown). Asymmetry in *FG/cortical rigidity* could arise from a preferred anterior localization of cortical actin or associated factors as found in other systems, for example, in the asymmetric division of *Drosophila* neuroblasts (McCartney et al., 1999). Another possibility is that MTs may target FGs to the cortex (Gupta et al., 2006). As we observe no significant difference in the number of MTs contacting the cortex on the anterior and posterior, similar amounts of FGs would then be delivered to both anterior and posterior cortices, which would be consistent with an asymmetry in the cortex rather than FG number.

Limitations of the Simulations

Many properties that are present in the embryo are not included in the simulation, leading to discrepancies. The smaller variation of oscillation periods, and the fact that the two poles oscillate with opposite phases in the embryo, is likely to be due to hydrodynamics effects, which are absent in cytosim. A clear indication that cytoplasmic flows are induced during oscillations is that yolk granules move with the spindle (Movie S11). During anaphase in the embryo, the spindle oscillation amplitude increases, and then decreases (Pecreaux et al., 2006), probably due to cell-cycle dependent changes, which are not considered in the simulation. However, these changes could be

reproduced, as parameter sensitivity analysis suggests that a gradual decrease in *FG attachment rate* or increase in *FG detachment rate* (Pecreaux et al., 2006), would lead to a loss of oscillations over time. Additional changes that occur in the embryo at the end of anaphase would require further extensions to our model; the invagination of the cleavage furrow changes the shape of the cell, and the flattening/disintegration of the posterior spindle pole (Hill and Strome, 1988) changes the distribution of microtubules.

Comparing In Silico and In Vivo Parameter Variations

Using the simulations, we performed two types of parameter variation. The first type involved changing all of the parameters of the simulation, in order to find parameter sets that allow the aster to oscillate as observed in vivo. We found that, in order to maintain oscillations, the parameters have to be such that oscillation speed is lower than MT growth speed. This was also observed in 24 live embryos, grown and analyzed at different temperatures. Temperature likely affects several parameters of the system at once, in addition to MT growth. At all temperatures examined, the in vivo posterior pole oscillated at speeds that were close to the maxima predicted by our model at each of the corresponding experimentally determined MT growth rates, although the simulation predicts only an upper, and not a lower limit, for oscillation speed. It is unclear whether there would be any benefit for the embryo to maximize oscillation speed (see below).

For analysis, we selected two parameter reference sets, where unknown values were chosen because they produced fast but stable oscillations, as in the embryo. Because multiple parameter sets fulfilled this criteria, values given for the unmeasured parameters in the parameter table should not be interpreted as estimates for cellular values. In the parameter sensitivity analysis, we assumed that the qualitative conclusions apply to the oscillation mechanism. Indeed, while the values of each parameter set are not identical, the shapes of the curves in response to parameter variation were similar. We may also compare the effect of single parameter variation in the simulations to an in vivo knock-down in a particular gene, because most of the parameters are tangible characteristics of the molecular players. In the future, it could be experimentally confirmed that regulators of MT dynamics modulate spindle pole oscillations, as predicted by simulations.

Oscillations Are Less Robust than Posterior Displacement

The parameter sensitivity analysis showed that changes to some parameters, notably MT growth and shrinkage speeds, lead to abrupt loss of oscillations, but only a gradual change in spindle pole displacement. This is consistent with the result of RNAi rundown of FG activity (Pecreaux et al., 2006), and with the results of a dynein temperature-sensitive mutant, that eliminated spindle pole oscillations, but not spindle displacement (Schmidt et al., 2005). Indeed, posterior displacement of the spindle seems more important for the survival of the embryo. However, spindle pole oscillations may not be without function. The oscillations initially occur in the plane perpendicular to the A-P axis, probably due to a smaller viscous resistance in that direction (motion along the A-P axis drags two asters, instead of only one for perpendicular motion). It may be that the oscillations stabilize the A-P positioning, in other words, absorb the intrinsic instabilities of cortical pulling. These ideas are interesting from a theoretical as well as a biological point of view, and could be investigated further in the future.

The model put forward arose from exploring the bases of cortical pulling through computer simulations. Our early investigations identified a complex relationship between MT dynamics, cortical contact and pulling forces. They showed that the dynamics of MTs at the cortex were fundamental in the positioning process, and led us to design the imaging experiments. The experiments, in turn, indicated the importance of MT flexibility. The model makes testable hypotheses on how the system should behave in response to changes to single or multiple parameters, in a way that can be verified with mutants and RNA interference.

EXPERIMENTAL PROCEDURES

Strains

C. elegans embryos were cultured as described (Grill et al., 2001). The transgene encoding the N-terminal YFP::α-tubulin (C47B2.3) fusion protein is under the control of the *pie-1* promoter; transgenic worms were created by microparticle bombardment (BioRad), as described (Praitis et al., 2001; Schlaitz et al., 2007). The TH65 YFP::α-tubulin and TH66 EBP-2::GFP worm strains were maintained at 25°C and imaged at 20.0 ± 1.0°C, unless otherwise stated.

Confocal Microscopy

Confocal images of embryos were obtained with a spinning disk confocal microscope (Zeiss Axioplan using a 63x 1.4 NA Plan Apochromat objective and Yokogawa disk head) with temperature control as in (Srayko et al., 2005). A 488nm Argon ion laser (Melles Griot) was used for illumination. Images were acquired with a Hamamatsu Orca ER 12 bit digital camera, at 500, 400, or 250 msec intervals, with either no binning or 2x2 binning. Images were processed in ImageJ, MATLAB and MetaMorph with custom macros, available upon request.

For imaging at the cortex and in the transverse plane, embryos were prepared using a hanging-drop method, whereby embryos in buffer are attached to the underside of a poly-lysine coated coverslip and transferred to a slide chamber to allow the embryo to hang freely. The stages of the embryo were followed by DIC. Metaphase-anaphase transition was detected by a slight elongation of the spindle poles. At this stage, the focus of the microscope was shifted to the cortex, and acquisition in the fluorescent channel was initiated. After 80 s of imaging, DIC imaging was resumed at the center of the embryo, to confirm that cell division occurred as normal, and to determine the anterior and posterior poles.

Number of MTs Contacting the Cortex

We estimated the density of MTs in the imaging plane (0.13 ± 0.03 dots/μm^2, mean and SD calculated from 21 embryos) by dividing the number of YFP::α-tubulin dots in a cortical movie (51.8 ± 19.3 dots, with 26.7 ± 10.0 dots on the anterior, 25.2 ± 10.1 dots on the posterior) by the imaged area (381.6 ± 74.8 μm^2). Assuming an ellipsoid embryo, the total surface area would be approximately $50 \times 30 \times \pi = 4700\ \mu m^2$.

Thus, there should be about 4700 × 0.13 = 613 ± 165 MTs within ~1 μm from the cortex. If we assume that the contact time is 1 s, out of the 4.1 s residency time, we obtain ~150 MTs actually contacting the cortex. The same calculation with 7 EBP-2::GFP embryos gives 210 MTs contacting the cortex.

Simulations

MT asters nucleated by centrosomes are simulated as in (Nedelec, 2002) using overdamped Langevin equations to describe the motion of elastic fibers in a viscous fluid, in the presence of Brownian motion. The cytoplasm is considered immobile and of constant viscosity. All stochastic events (FG binding, catastrophes, nucleation) are generated as first-order random events, *i.e.* with a constant probability of occurrence.

Centrosomes, Asters and Spindle

Centrosomes are modeled as spheres (or a circle in 2D) of radius 1 μm with 300 points regularly distributed on the surface. To make an aster, a sphere is linked mechanically to two points on each fiber, with Hookean links of stiffness 1000 pN/μm, between the center and the MT minus-end, and between the point on the surface and the point 1 μm distal on the fiber. The sphere may rotate and translate in space under the effect of MT forces transmitted by the centrosome-links.

In the embryo, the two asters are linked by the mitotic spindle, which constrains them in their motions. In the 3D simulation, MT fibers that grow toward the opposite pole, at an angle of less than 45 degrees from the axis, were removed and replaced by a single rigid mechanical element of 2 μm thickness representing the spindle. This element, which lengthens at constant speed, constrains the distance between the pole and their relative orientation.

Microtubules

The MTs in a fiber grow and shrink at constant speeds. Catastrophe events occur according to two rates, depending on whether the plus-end of the MT is in contact with the cortex or not. When MTs hit the cortex they also grow slower, according to the measured reduction of tubulin assembly on MTs that experience force on their plus-end (Janson et al., 2003). However, the effect of this assumption is slight, since MTs depolymerize quickly after making cortical contacts. After a catastrophe event, if the MT shrinks all the way, it liberates a nucleation site on the centrosome. The number of nucleation sites was set at 15/fiber. A free nucleation site may produce a new MT at a rate of 0.05/s.

Fibers: Microtubule association

In the reference simulation, each of the 300 fibers represents a group of MTs. Because of the nucleation rate, the number of MTs per fiber is variable, but was on average 6/fiber. These values are somewhat arbitrary, as for example 200 fibers each containing on average 9 MTs/fiber gave similar results (data not shown). The rigidity of the fibers is difficult to estimate, because it depends not only on the rigidity of individual MTs, measured in vitro to be about 20–40 pN μm^2 (Dogterom and Yurke, 1997), but also on their association and relative length. Here, we used *fiber rigidity* ~120 pN μm^2.

MT association had one important effect: MTs in a fiber always contact the cortex at approximately the same position (see Figure 4B), because the viscosity is such that the fiber plus-tip hardly moves laterally during the oscillation time. In the reference simulation, the time for a fiber to straighten $\tau \approx$ *viscosity* (*fiber length*)^4/(*fiber rigidity*) ≈ 420 s is longer than the oscillation period of ~25 s. Thus the measured cytoplasmic viscosity (Daniels et al., 2006) is sufficient to explain the observation that fibers always contact the cortex at the same position. Entanglements with organelles would reinforce the effect.

Cell Cortex

The simulated cell is a cylinder capped with 2 hemispheres. The simulation includes a confinement force that is linear to the extent by which a MT protrudes outside the volume. This interaction can be turned off in the simulation with little effect (Figure S2B).

Force Generators

The FGs are able to capture fiber tips that touch the cortex, with a probability *FG attachment rate,* which incorporate the density of FGs in the cortex and their binding rate to MTs. A new FG is created and fixed on the membrane at the initial point of contact. When a captured MT shrinks and recedes from the cortex, the FG produces a pulling force, which is proportional to the stretch required to link the cortex and the plus-end, **F** = (*FG/cortical rigidity) (position on cortex – position of fiber tip)*. The FG/cortical rigidity includes the *elasticity* of the molecular link and the *rigidity* of the cortex itself. The shrinking speed of the MT is unchanged. Detachment soon follows, because the detachment rate k_{off} of the FGs increases with force **F**, as k_{off} = *(detachment rate)* exp(**F**/*characteristic force*), according to Kramer's theory. Any detached FG is deleted from the simulation. Together with the linear relationship between force and stretch, Kramer's law can result in more force being produced when the rigidity is lower. This explains why a softer posterior cortex may lead to posterior displacement.

Supplemental Data

Supplemental Data include Supplemental Experimental Procedures, Supplemental References, six figures, and eleven movies and can be found with this article online at http://www.cell.com/cgi/content/full/129/3/499/DC1/.

ACKNOWLEDGMENTS

We thank T. Hyman, in whose laboratory the experimental data were collected, for his generosity and advice on the project; S. Blandin, S. Grill, J. Howard, F. Jülicher, M. Kaksonen, and T. Surrey for discussions and comments on the manuscript; members of the Nedelec lab involved in the development of cytosim; and IBM for generous hardware support. We thank our referees, in particular for the suggestion to try different rigidities on the A/P cortices. F.N. is supported by BioMS, an initiative from the Klaus Tschira Foundation, and acknowledges research grant RGY84 from HFSP. C.K. is supported by an "E-STAR" fellowship funded by the EC's FP6 Marie Curie Host fellowship for Early Stage Research Training under contract number MEST-CT-2004-504640.

Received: August 25, 2006
Revised: December 1, 2006
Accepted: March 2, 2007
Published: May 3, 2007

REFERENCES

Adames, N.R., and Cooper, J.A. (2000). Microtubule interactions with the cell cortex causing nuclear movements in Saccharomyces cerevisiae. J. Cell Biol. *149*, 863–874.

Albertson, D.G. (1984). Formation of the first cleavage spindle in nematode embryos. Dev. Biol. *101*, 61–72.

Carminati, J.L., and Stearns, T. (1997). Microtubules orient the mitotic spindle in yeast through dynein-dependent interactions with the cell cortex. J. Cell Biol. *138*, 629–641.

Colombo, K., Grill, S.W., Kimple, R.J., Willard, F.S., Siderovski, D.P., and Gonczy, P. (2003). Translation of polarity cues into asymmetric spindle positioning in Caenorhabditis elegans embryos. Science *300*, 1957–1961.

Cowan, C.R., and Hyman, A.A. (2004). Asymmetric cell division in C. elegans: cortical polarity and spindle positioning. Annu. Rev. Cell Dev. Biol. *20*, 427–453.

Daniels, B.R., Masi, B.C., and Wirtz, D. (2006). Probing single-cell micromechanics in vivo: the microrheology of C. elegans developing embryos. Biophys. J. *90*, 4712–4719.

Dogterom, M., Kerssemakers, J.W., Romet-Lemonne, G., and Janson, M.E. (2005). Force generation by dynamic microtubules. Curr. Opin. Cell Biol. *17*, 67–74.

Dogterom, M., and Yurke, B. (1997). Measurement of the force-velocity relation for growing microtubules. Science *278*, 856–860.

Gonczy, P. (2002). Mechanisms of spindle positioning: focus on flies and worms. Trends Cell Biol. *12*, 332–339.

Gotta, M., Dong, Y., Peterson, Y.K., Lanier, S.M., and Ahringer, J. (2003). Asymmetrically distributed C. elegans homologs of AGS3/PINS control spindle position in the early embryo. Curr. Biol. *13*, 1029–1037.

Grill, S.W., Gonczy, P., Stelzer, E.H., and Hyman, A.A. (2001). Polarity controls forces governing asymmetric spindle positioning in the Caenorhabditis elegans embryo. Nature *409*, 630–633.

Grill, S.W., Howard, J., Schaffer, E., Stelzer, E.H., and Hyman, A.A. (2003). The distribution of active force generators controls mitotic spindle position. Science *301*, 518–521.

Grill, S.W., and Hyman, A.A. (2005). Spindle positioning by cortical pulling forces. Dev. Cell *8*, 461–465.

Grill, S.W., Kruse, K., and Julicher, F. (2005). Theory of mitotic spindle oscillations. Phys. Rev. Lett. *94*, 108104.

Grishchuk, E.L., Molodtsov, M.I., Ataullakhanov, F.I., and McIntosh, J.R. (2005). Force production by disassembling microtubules. Nature *438*, 384–388.

Gupta, M.L., Jr., Carvalho, P., Roof, D.M., and Pellman, D. (2006). Plus end-specific depolymerase activity of Kip3, a kinesin-8 protein, explains its role in positioning the yeast mitotic spindle. Nat. Cell Biol. *8*, 913–923.

Hill, D.P., and Strome, S. (1988). An analysis of the role of microfilaments in the establishment and maintenance of asymmetry in Caenorhabditis elegans zygotes. Dev. Biol. *125*, 75–84.

Howard, J. (2006). Elastic and damping forces generated by confined arrays of dynamic microtubules. Physical Biology *3*, 1478–3975.

Inoue, S., and Salmon, E.D. (1995). Force generation by microtubule assembly/disassembly in mitosis and related movements. Mol. Biol. Cell *6*, 1619–1640.

Janson, M.E., de Dood, M.E., and Dogterom, M. (2003). Dynamic instability of microtubules is regulated by force. J. Cell Biol. *161*, 1029–1034.

Kemphues, K.J., Priess, J.R., Morton, D.G., and Cheng, N.S. (1988). Identification of genes required for cytoplasmic localization in early C. elegans embryos. Cell *52*, 311–320.

Labbe, J.C., Maddox, P.S., Salmon, E.D., and Goldstein, B. (2003). PAR proteins regulate microtubule dynamics at the cell cortex in C. elegans. Curr. Biol. *13*, 707–714.

Manneville, J.B., and Etienne-Manneville, S. (2006). Positioning centrosomes and spindle poles: looking at the periphery to find the centre. Biol. Cell. *98*, 557–565.

McCarthy, E.K., and Goldstein, B. (2006). Asymmetric spindle positioning. Curr. Opin. Cell Biol. *18*, 79–85.

McCartney, B.M., Dierick, H.A., Kirkpatrick, C., Moline, M.M., Baas, A., Peifer, M., and Bejsovec, A. (1999). Drosophila APC2 is a cytoskeletally-associated protein that regulates wingless signaling in the embryonic epidermis. J. Cell Biol. *146*, 1303–1318.

Munro, E., Nance, J., and Priess, J.R. (2004). Cortical flows powered by asymmetrical contraction transport PAR proteins to establish and maintain anterior-posterior polarity in the early C. elegans embryo. Dev. Cell *7*, 413–424.

Nedelec, F. (2002). Computer simulations reveal motor properties generating stable antiparallel microtubule interactions. J. Cell Biol. *158*, 1005–1015.

Pecreaux, J., Roper, J.C., Kruse, K., Julicher, F., Hyman, A.A., Grill, S.W., and Howard, J. (2006). Spindle Oscillations during Asymmetric Cell Division Require a Threshold Number of Active Cortical Force Generators. Curr. Biol. *16*, 2111–2122.

Praitis, V., Casey, E., Collar, D., and Austin, J. (2001). Creation of low-copy integrated transgenic lines in Caenorhabditis elegans. Genetics *157*, 1217–1226.

Schlaitz, A.L., Srayko, M., Dammermann, A., Quintin, S., Wielsch, N., MacLeod, I., de Robillard, Q., Zinken, A., Yates, J.R., III, Muller-Reichert, T., et al. (2007). The *C. elegans* RSA complex localizes protein phosphatase 2A to centrosomes and regulates mitotic spindle assembly. Cell *128*, 115–127.

Schmidt, D.J., Rose, D.J., Saxton, W.M., and Strome, S. (2005). Functional analysis of cytoplasmic dynein heavy chain in Caenorhabditis elegans with fast-acting temperature-sensitive mutations. Mol. Biol. Cell *16*, 1200–1212.

Srayko, M., Kaya, A., Stamford, J., and Hyman, A.A. (2005). Identification and characterization of factors required for microtubule growth and nucleation in the early C. elegans embryo. Dev. Cell *9*, 223–236.

Strome, S., Powers, J., Dunn, M., Reese, K., Malone, C.J., White, J., Seydoux, G., and Saxton, W. (2001). Spindle dynamics and the role of gamma-Tubulin in early Caenorhabditis elegans embryos. Mol. Biol. Cell *12*, 1751–1764.

Toba, S., Watanabe, T.M., Yamaguchi-Okimoto, L., Toyoshima, Y.Y., and Higuchi, H. (2006). Overlapping hand-over-hand mechanism of single molecular motility of cytoplasmic dynein. Proc. Natl. Acad. Sci. USA *103*, 5741–5745.